Tribology Letters, Vol. 26, No. 1, April 2007 (© 2007)
DOI: 10.1007/s11249-006-9191-8

A predictive analytical friction model from basic theories of interfaces, contacts and dislocations

A. P. Merkle and L. D. Marks*

Department of Materials Science and Engineering, Northwestern University, Evanston, IL 60208, USA

Received 8 September 2006; accepted 18 December 2006; published online 7 February 2007

Friction between crystalline bodies is described in a model that unifies elements of dislocation drag, contact mechanics, and interface theory. An analytic expression for the friction force between solids suggests that dislocation drag accounts for many of the observed phenomena related to solid–solid sliding. Included in this approach are strong arguments for agreement with friction dependence on temperature, velocity, orientation, and more general materials selection effects. It is shown that calculations of friction coefficients for sliding contacts are in good agreement with available experimental values reported from ultrahigh vacuum experiments. Extensions of this model include solutions for common types of dislocation barriers or defects. The effects of third-body solid lubricants, superplasticity, superconductivity, the Aubry transition, and supersonic dislocation motion are all discussed in the framework of dislocation-mediated friction.

KEY WORDS: friction mechanisms, dislocations, interfaces, solid lubrication friction, nanotribology

1. Introduction

The laws of friction dating back to DaVinci, Coulomb, and Amontons still see use in basic discussions of the phenomenon [1]. Three basic observations have persisted for 100s of years: the dependence of the friction force on normal load, the independence of friction with velocity and with apparent area of contact. Unfortunately, none of these laws are universally valid; more importantly, nothing fundamental about the dissipative processes associated with friction may be derived from these basic expressions [2]. Nanotribological friction experiments capable of single asperity analysis, enabled by the development of tools with high force sensitivities such as the atomic force microscope [3,4] (AFM), quartz crystal microbalance [5,6] (QCM), and the surface force apparatus (SFA) [7], have shown that the macroscopic friction laws are not the same as the atomic (nanoscale) origins of friction.

The atomic origins of friction have been the subject of theoretical studies since the introduction of Tomlinson's model [8] of a ball and spring dragged over a periodic potential. This model and its successors including the Frenkel–Kontorova [9] model produced a number of successful solutions for interfaces including stick slip behavior in friction [10], the formation of misfit dislocations [11,12] and more general commensurability effects in static [13] and kinetic cases [10]. Unfortunately in most cases these models describe static friction, and do not always include the dissipative terms, which lead to dynamic friction. More recently, numerical methods, such as molecular dynamics have studied atomic scale friction phenomena on short time and length scales [14,15].

Consider the *gedanken* case of forming an interface between two grains (of the same or different materials) of periodic materials by placing cut sections of the perfect lattices in contact. At the interface there will be unbalanced stresses due to the mismatch of the two lattices. In almost all cases, these are relieved by the formation of dislocations near the interface; this is true independent of whether we are talking about metals, ceramics, or crystalline polymers (e.g., self-assembled monolayers). Note that these dislocations are intrinsic to the presence of the boundary, and are not introduced by any external action such as deformation. Suppose we now apply a shear stress across the interface as in a friction experiment. Relative sliding can occur via:

(a) Motion of dislocations near the interface
(b) Motion of dislocations away from the interface
(c) Rigid body translations of the two materials as in a Tomlinson model.

It is well known that in general mode (c) requires much higher stresses than either (a) or (b); plastic deformation is almost always achieved via dislocation motion. If the interface is relatively weak compared to the bulk material the low energy path will almost always be (a). The dominant dissipative forces associated with

*To whom correspondence should be addressed.
E-mail: l-marks@northwestern.edu

the motion of dislocations are well documented in the literature [16].

The purpose of this paper is to develop a general model for friction considered in terms of the dissipative forces on the interfacial dislocations. This friction model is solved analytically from first principals, combining elements of three independently well-known physical theories: interface theory, dislocation dynamics and contact mechanics. Strictly speaking, the model only applies to the unique case of a perfectly flat interface. However, since the model is analytical (not numerical) it can be used to extract general trends. Furthermore it is quite plausible to extend the model to more experimentally realistic cases, such as when there are barriers to dislocation motion near the interface, using well-established existing information about dislocations.

We will first take a look at each of these theories independently so that the combined model may be understood from a common viewpoint. We acknowledge that large parts of these fields are well established, but it is nonetheless useful to summarize them here, realizing that despite their diverse origins, they may collectively play an important role in the study of friction at the nanoscale. General discussion is available in the literature regarding the theories of interfaces [17–19], dislocations [20,21], and contact mechanics [22–24].

2. Interface theory and the geometry of interfacial dislocations

We need to understand the geometry and density of interfacial dislocations. The standard approach is based upon the coincident site lattice (CSL) theory developed by Bollmann [25,26] and Grimmer [27], as a geometric model describing the coincidence, or "goodness of fit" of atomic lattice sites at an interface. To introduce the basics of CSL theory, imagine two parallel perfect atomic lattices are brought into contact. The two structures are considered perfectly coincident if each lattice site directly mirrors its counterpart through the interfacial plane (figure 1). This, of course, is an exceedingly rare condition, and for a given in-plane rotation of one of the surfaces (known as a twist boundary, figure 2) most of the lattice sites will fall out of coincidence with the opposing surface. However, some small fraction of atomic sites will be shifted into coincidence forming a unique periodic structure, as depicted in figure 1 for the $\sum 5$ CSL. This periodic arrangement can be mathematically described as a two-dimensional lattice, where the inverse fraction of sites in coincidence relative to the total number of real projected interfacial atomic sites is represented by its $\sum$ value. Hence, a $\sum 5$ (figure 1) coincident site twist boundary has 1/5th of the total number of interfacial atoms in coincidence and results from an in-plane misorientation of 36.87 degrees.

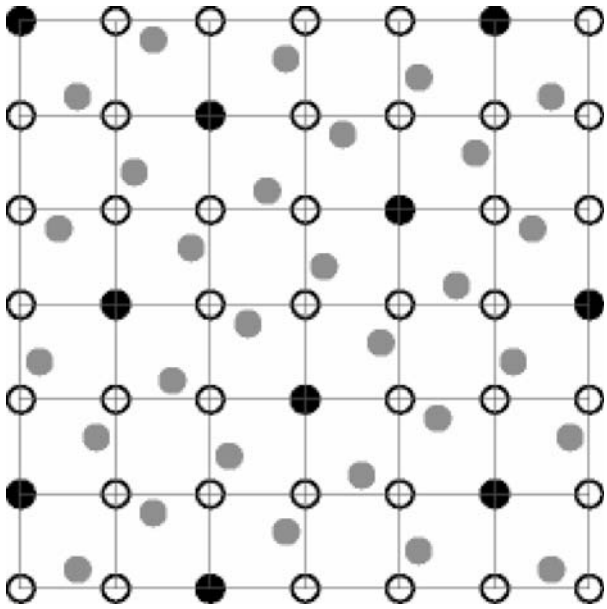

Figure 1. Plan view of an unrelaxed $\Sigma 5$ coincident site lattice ($\theta = 36.87°$) produced by the relative in-plane misorientation of two parallel cubic lattices. Open (grey) circles correspond to the top (bottom) lattice, and black sites indicate perfectly coincident registry between the top and bottom planes.

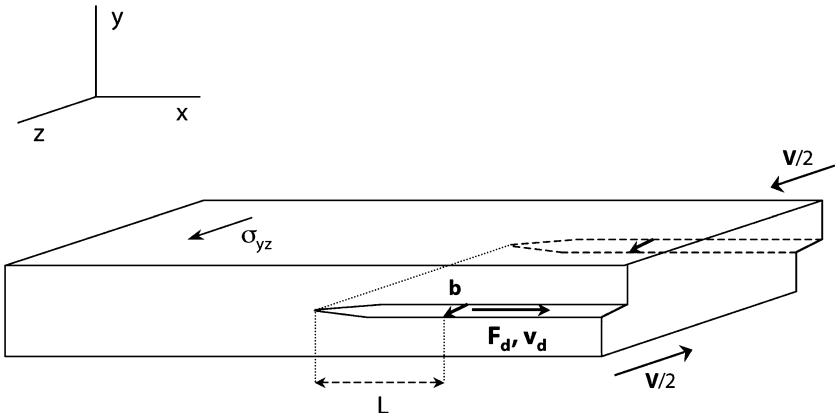

Figure 2. Force experienced by a screw dislocation resulting from an interfacial shear.

Table 1.
The five most coincident twist boundary CSL arrangements for cubic lattices and their corresponding misorientation angles.

Sigma	Misorientation angle (degrees)
1	0
5	36.9
13	22.6
17	28.1
25	16.3

For real non-rigid interfaces, boundary dislocations will form to accommodate lattice strain. Between dislocations, interfaces tend to form structures that match low $\sum$ values. Although the exact relationship between the degree of coincidence and grain boundary energy is unknown, it is generally accepted that higher coincidence yields lower energy boundaries. In fully relaxed cases, interfaces are energetically preferred at slight misorientations inducing periodically spaced dislocations relative to exact low index boundary configurations (Table 1). This corresponds to an energetic balance between regions of perfect $\sum$ registry separated by small regions of misfit at grain boundary dislocations. For the case of twist grain boundaries (in-plane misorientation), Frank's formula [21] describes the dislocation separation distance L for a given misfit angle, θ:

$$L = \frac{|\mathbf{b}|}{2\sin(\Delta\theta/2)}, \tag{1}$$

where $\Delta\theta$ is the angular increment away from a perfect $\sum$ boundary orientation.

3. Dissipative forces for a moving dislocation

We now turn to the dissipative forces for a moving dislocation. Early investigations into the sources of dislocation drag considered the main source to be associated with phononic dissipative processes. Originally [28], it was suggested that the motion of dislocations should follow a standard viscous force model, with drag directly proportional to velocity. As experimental evidence for nonlinear mobility of dislocations emerged [29,30], it became clear that a viscous model could in no way completely describe the dynamics of dislocations. Now it is understood that several mechanisms influence the mobility of dislocations through a solid, and that competition between thermal fluctuations and dynamic radiative processes takes place [16,29,30].

Most phonon contributions to dislocation drag behave viscously, that is, with direct proportionality to the velocity. They can be described by a drag coefficient, B, having the following relation:

$$F = Bv, \tag{2}$$

where B is the total drag coefficient and $\mathbf{v}$ is the dislocation velocity. More accurately, this expression should read

$$F_i = B_{\mathrm{ij}}.v_j, \tag{3}$$

where the drag coefficient is a tensor quantity, and contains anisotropic effects. B will be expressed as a sum of number of viscous drag effects.

The first phononic mechanism, known as the "phonon wind", arises from an aberrational effect associated with a phonon distribution in a moving reference frame. Phonons are scattered by moving dislocations as a result of the nonlinear elastic properties of the crystal. The expression for the damping coefficient of a screw dislocation by the phonon wind [31] is

$$B_{\mathrm{w}} = \frac{1+\left(3+\frac{n}{2\mu}\right)^2}{\pi^2}\frac{\hbar}{b^3}\left(\frac{bk\Theta}{3\hbar c_{\mathrm{t}}}\right)^5 f\left(\frac{T}{\Theta}\right), \tag{4}$$

where μ is the shear modulus, b is the magnitude of the Burgers vector, k is the Boltzmann constant, c_{t} is the shear wave velocity, n is a Murnaghan coefficient, and Θ is the Debye temperature. $f(x)$ is a more complex function of temperature, and is expressed for screw dislocations as

$$f(x) = x^5\int_0^{1/x} dt\frac{t^5e^{\mathrm{t}}}{(e^{\mathrm{t}}-1)^2}. \tag{5}$$

In the limiting case of $T \gg \Theta$, B_{w} becomes

$$B_{\mathrm{w}} = \frac{b}{\pi^2 c_{\mathrm{t}}}\left(\frac{3kT}{b^3}\right)\left[\frac{1+\left(3+\frac{n}{2\mu}\right)^2}{36}\left(\frac{bk\Theta}{3\hbar c_{\mathrm{t}}}\right)^4\right]. \tag{6}$$

Since a dislocation within a crystal contains its own degrees of freedom, it may vibrate in the thermal motion of the lattice and consequently radiate elastic waves. This is known as the "flutter" effect [2], and is expressed by

$$B_{\mathrm{fl}} = \frac{\hbar k_{\mathrm{D}}^3}{\pi^2} f\left(\frac{T}{\Theta}\right), \tag{7}$$

where k_{D} is the upper limit to the Debye spectrum, and f is yet another complex function [32] of temperature. For a description of this temperature term, we direct the reader to a work by Alshits [32]. The "flutter" effect is a re-radiation of phonons oscillating in a thermal lattice field and will dominate over the phonon wind (nonlinear scattering) mechanism at low temperatures and in materials with a low degree of anharmonicity.

Interactions with phonons are not the sole source of energy dissipation for moving dislocations. An expression for the electronic damping of dislocations was solved by Holstein [33] to be

$$B_e \cong \frac{bN_e\varepsilon_F}{10v_F}, \tag{8}$$

where N_e is the number of conduction electrons, ϵ_F is the Fermi energy, and v_F is the Fermi velocity. Typically, this value is not significant at room temperature where phonon effects dominate. However, when low enough temperatures are reached where phonon modes are frozen out and where the free electron density is sufficiently high, this term can be on the same order as the total phonon contribution [16]. However the story is not quite that simple, since low temperatures necessitate the consideration of the superconducting transition. The effect on mobility of dislocations traveling through bulk solids by superconductivity has been observed experimentally [34–38] and predicted theoretically [39], and we expect it to manifest itself in the case of solid friction.

The phonon wind, flutter, and electronic drag mechanisms are the principal viscous drag contributors to dislocations moving through a solid. Another mechanism, radiation friction, plays a dominant role particularly at low velocities, where friction studies are most relevant. The discreetness of the atomic lattice means that the strain field associated with a moving dislocation oscillates with time, and elastic waves radiate from the configurational oscillations of the dislocation core. Even at 0 K, when all other dissipative channels are eliminated, this effect remains strong. Alshits [40] solved a stabilized solution by including the previously determined viscous drag terms into the form

$$F = \sigma_p b \coth\left[\frac{b\sigma_p}{B_{tot}v_d}\right], \tag{9}$$

where σ_p is the Peierls stress and B_{tot} is the viscous drag coefficient. B_{tot} can be broken down linearly into its individual components (phononic and electronic) as described above:

$$B = B_e + B_w + B_{fl}. \tag{10}$$

Consistent with the phenomenon of static friction, the total radiation drag stress will approach σ_p at zero velocity.

4. Calculating the true area of contact

The dissipative forces only apply over the true contact area, a standard problem in contact mechanics. The Hertzian contact area, A, between a plane and a sphere follows a load, L, dependence

$$A = \pi\left(\frac{RL}{E'}\right)^{\frac{2}{3}}, \tag{11}$$

where R is the radius of the sphere, and E' is the effective modulus given by

$$\frac{1}{E'} = \frac{4}{3}\left(\frac{1-\nu_1^2}{E_1} + \frac{1-\nu_2^2}{E_2}\right), \tag{12}$$

where E_1 and E_2 and ν_1 and ν_2 are the Young's modulus and Poisson's ratios of the two materials, respectively. Despite finding somewhat reasonable agreement on a macroscopic scale, the theory underestimates the contact area for microscopic contacts since it ignores adhesion. This is compensated for in solutions by Johnson, Kendall and Roberts [41] (JKR), and Derjaguin, Müller and Toporov [42] (DMT).

No macroscopic surface is perfectly smooth, and therefore a number of small asperities are responsible for contacting a relatively small fraction of the apparent projected area. This is satisfied to some degree through models established by Greenwood *et al.* [43, 44], but remains an active field of research.

5. Model

Now that we have established the fundamental theories related to the contact of crystalline bodies, we turn to the specific development of the proposed model for interfacial solid friction. Consider an interface between two materials in terms of an array of misfit dislocations of Burgers vector **b** with a nearest-neighbor separation of L. The separation, L, is determined by the periodicity and relative orientation of the two contacting surfaces. If the two bodies are in relative motion with a velocity, **V**, the dislocation velocity, v_d, in turn will be:

$$v_d = L\mathbf{b}\cdot\mathbf{V}/b^2. \tag{13}$$

This proportionality arises from the geometric condition that requires a single screw dislocation to be punched out one interdislocation length after an orthogonal surface displacement of one burgers vector, as illustrated in figure 2. The motion of a dislocation with burgers vector, **b,** and line vector, ξ, will follow the Peach–Koehler relation: $\mathbf{F} = (\mathbf{b}\cdot\sigma)\times\xi$, where σ is the applied shear stress, and will move in a direction normal to the burgers vector**.** For the case of pure misfit dislocations in a cubic twist boundary, the burgers vector distribution is in-plane and orthogonal to one another (figure 3). Due to this intersecting distribution, a cosine (dot product) dependence on the drag force results from

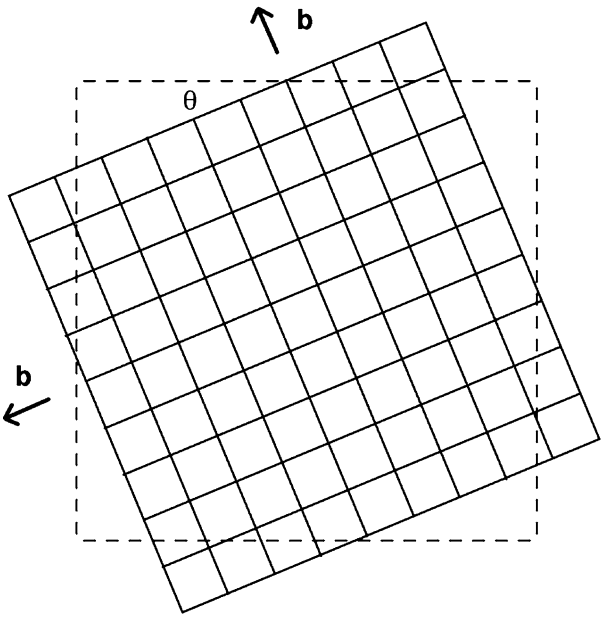

Figure 3. Plan view of a dislocation network produced by a twist grain boundary. Burgers vectors, **b**, exist at right angle to each other, in plane with the interface. Small deviations in misfit angle will produce significant changes in the interdislocation spacing.

changing the sliding direction. Only dislocations with burgers vector components in the direction of sliding experience a drag force.

The expression for the velocity of the interfacial dislocations (equation 13) is substituted into the radiation dragging term (equation 9). Frank's equation (equation 1) for the dislocation spacing, L, is also substituted into equation 9; converting back to the retarding force that needs to be overcome for continuing motion at the macroscopic level (accounting for the arrangement of dislocations in a twist boundary) gives

$$F_{\text{macro}} = \frac{N_{\text{d}}\gamma(\sigma_{\text{p}}b)}{2}\coth\left(\frac{2(\sigma_{\text{p}}b)\sin(\Delta\theta/2)}{B_{\text{tot}}V}\right), \quad (14)$$

where $\gamma = \sin(\theta) + \cos(\theta)$, N_{d} is the number of dislocations in the contact area, θ is the absolute in-plane misorientation angle and $\Delta\theta$ is the angular displacement from a given coincident site orientation (Σ boundary). γ represents the orthogonal distribution of Burgers vectors in a lattice for a pure cubic twist boundary, and may readily be generalized for tilt or more complicated boundaries. Tilt boundaries containing edge dislocations have not been calculated here, but will follow the same model formulation. It necessitates a geometric transformation accounting for the dislocation distribution (Frank's formula) and a reevaluation of the viscous and radiation drag terms. The viscous terms for edge-type dislocation drag are known and will change slightly in magnitude and temperature dependence; the more significant consideration requires an analysis of the core structure of the edge dislocation for radiation drag. The authors are unaware of a closed form analytical solution of this type.

One last step is needed to account for the true area of contact. In the analysis above we have considered perfect contact between the two bodies, but it is known that in reality a small number of asperities are in contact. The most basic definition for the friction coefficient can be written as

$$\mu = \frac{F_{\text{macro}}}{F_{\text{N}}}, \quad (15)$$

where the normal load F_{N}, will determine the dislocation array length A. The friction coefficient is only meaningful if specific geometric and materials parameters are known for the contact, since friction can vary significantly with load. Variation in calculated values for μ (static or kinetic) will result from the selection of different contact models, e.g., Hertzian, JKR, DMT, or through the choice of specific materials dependent factors as compliance and adhesion. For this reason, equation 15 is left in this general form, where F_{macro} depends on the dislocation density and the contact area as given by a chosen contact model.

6. Results

Figures 4 and 5 show the dependence of the macroscopic friction force (equation 14) on the dislocation velocity using the $\Sigma 1$ boundary. The calculations for figure 3 use experimental parameters given by McFadden for UHV sliding of Cu single crystals [45], while figure 5 demonstrates the effect of reducing the Peierls stress for Cu. The radiation friction term clearly dominates the friction force at low velocities, and the asymptotic convergence to the Peierls stress at zero velocity indicates that static friction exists for all cases where a Peierls-type barrier is present. The critical velocity knee, where viscous effects begin to dominate, is strongly dependent on the Peierls resistance and the temperature and can exist in bulk metals at significant fractions of the shear wave velocity. This critical velocity is small for systems that are weakly bound (sliding monolayers), shear easily in preferred crystallographic directions (graphite, MoS_2), or contain third body lubricating layers. It is worth noting that an exceedingly similar velocity dependence has very recently been observed for glassy polymethylmethacrylate and octadecyltrichlorosilane by Bureau *et al.*; in terms of the model used here it corresponds to a Peierls stress of 0.02–1 Pa which we believe is a reasonable number for a polymeric system [46].

To further illustrate the consequences of equation 14, figure 6 shows how the friction force, F_{macro}, varies as a function of misorientation angle for highly coincident boundaries. An anisotropic friction force shows increases in friction at misorientations consistent with CSL theory. The choice of CSL boundaries in figure 6 is

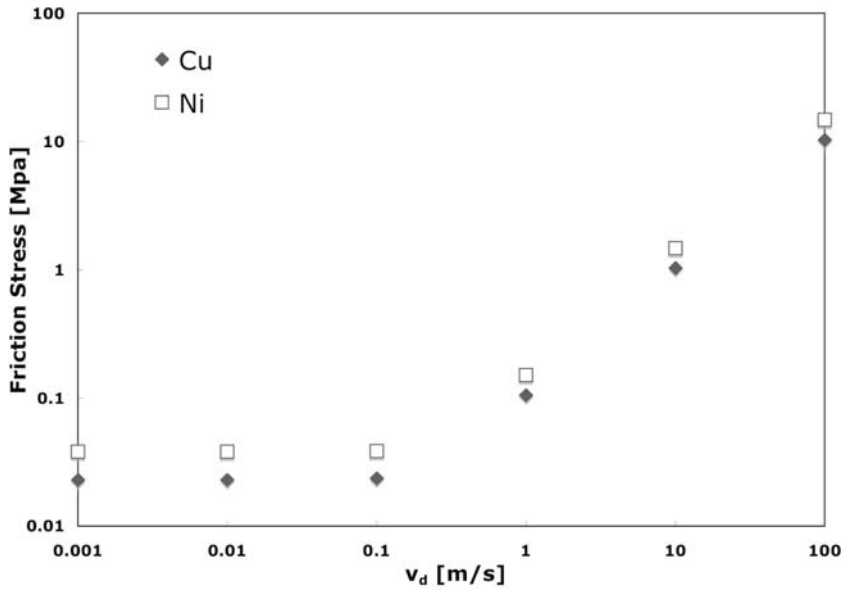

Figure 4. Frictional stress per dislocation as a function of dislocation velocity calculated at 100 K for Cu(111) and 300 K for Ni(100), following McFadden [45] and Ko [52]. The crossover point from pinned to viscous behavior is determined to be 0.1 m/s for the given set of conditions.

limited to the highest density of coincident site states. The determination of a cutoff in the number of peaks is not trivial, but experimental studies on (100) twist boundaries have confirmed the existence of unique dislocation networks as high as Σ41 [47]. At which point misorientations away from CSL boundaries will yield areas of higher coincidence remains a subtle and unanswered question.

Friction anisotropy is predicted in this model for both variations in sliding direction and misorientation (same sliding direction). For variations in sliding direction, the dislocation distribution, γ, contains this dependence, in agreement with other experimental and theoretical suggestions [48,49]. Experimental evidence [48, 50–53] for friction anisotropy exists for several different interfaces, but no general consensus exists as to the specific sliding conditions that yield this effect. Our model predicts that misorientation anisotropy increases with velocity, where viscous dislocation drag is the dominant retarding force. Solid–solid friction experiments should show an increase in anisotropic effects not only as load is increased, as in the study by Enomoto and Tabor [54], but as velocity passes the critical limit that yields to a dominant viscous dislocation drag

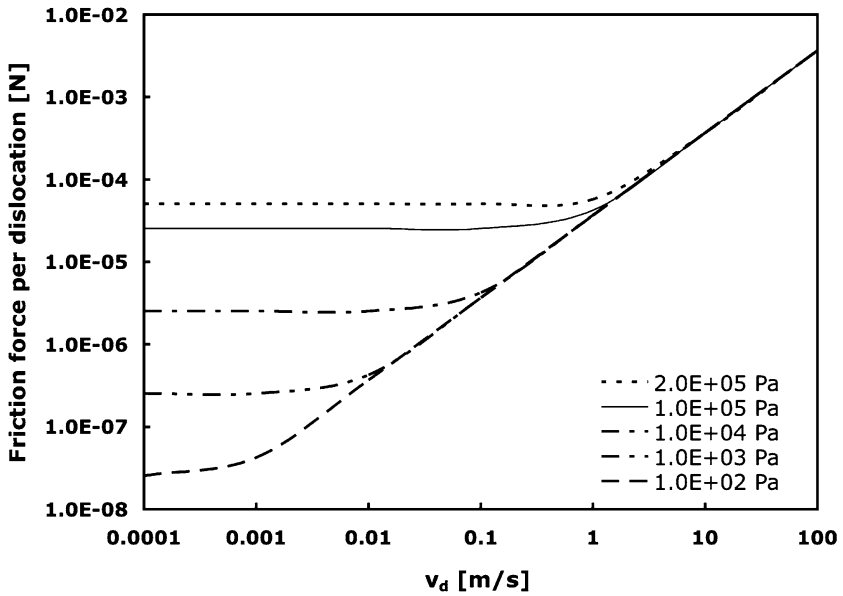

Figure 5. Drag force per dislocation plotted as a function of dislocation velocity for several Peierls stress values. All contact and sliding parameters follow those given in the Cu friction experiments by McFadden *et al.*

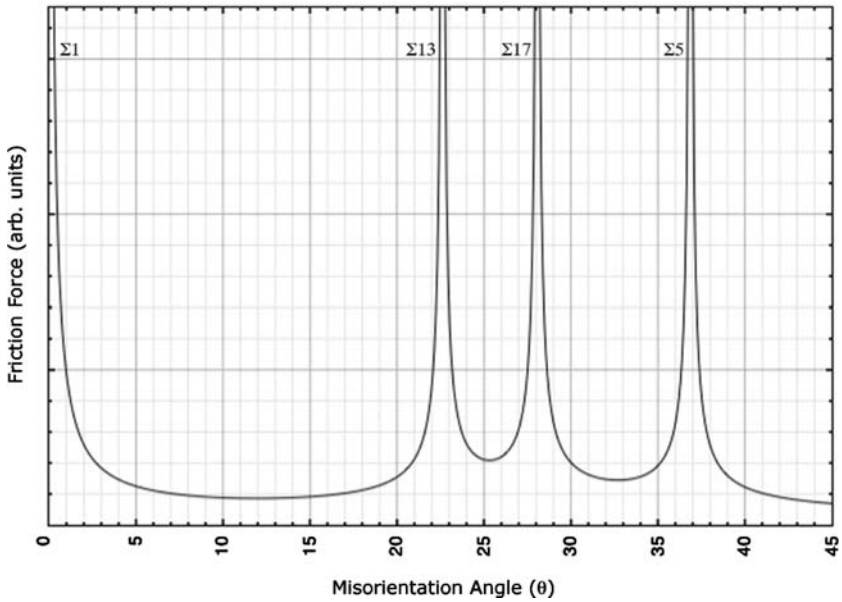

Figure 6. Friction as a function of twist misorientation angle. Only the lowest four CSL boundaries are shown.

regime. A tradeoff can be made for high velocity experiments by studying a system at higher temperatures or with a lower Peierls barrier resistance (sliding monolayers).

A graph of the temperature dependence of equation 14 is given in figure 7 for the case of Cu. Although the precise temperature dependence of the Peierls stress, $\sigma_p(T)$, is not known, it has been experimentally observed to decrease by an order of magnitude between 4.2 K and 300 K in close packed metals [55]. Competition exists at finite temperatures between increased viscous drag contributions that increase the required stress and an activation rate increase that lowers it. Landau derived the effective velocity of dislocations as a function of statistical thermal surmounting of randomly spaced Peierls barriers [56]. The inclusion of this velocity correction term $v_{\text{eff}} \sim ve^{\left(\frac{-\Delta H}{kT}\right)}$, where ΔH is the activation enthalpy estimated to be 0.01 eV and k is the Boltzmann constant, has a minimal effect on the radiation force term, where force is nearly constant with velocity. However, the correction is significant for the viscous dominated regime.

An important step in validating the present model is examining whether calculated friction forces match experimental data. Values are calculated for the macroscopic friction coefficient based on a limited number of available UHV friction studies. It must be stressed that the calculated values for μ are not universally

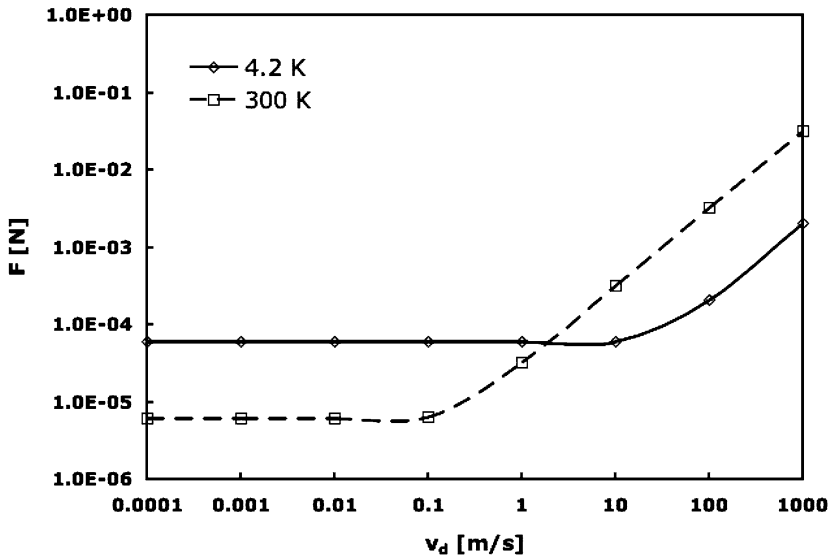

Figure 7. The effect of temperature on the shape of the radiation drag of dislocations calculated for Cu.

valid, rather they represent specific values calculated for the experimental conditions (load, tip shape, sliding velocity, environment, material) given in the referenced studies and fundamental materials constants. Upper and lower limits for the dislocation spacing, L, were taken from experimental results of TEM studies of manufactured twist grain boundaries [57–59]. Table 2 lists the values for μ as calculated by our analytical model and as reported in UHV friction experiments [45,52,60]. The experimental friction values fall within the model's calculated range; not only is there good absolute agreement, but relative changes in measured coefficients of friction between different metals are also accounted for. An increase in friction is present from Fe (lowest) to Ni (highest), and is directly predicted by the analytical calculations. Although, the range of values in table 2 vary from two to three orders of magnitude – something which is rarely seen experimentally – they represent upper and lower limits of ideal single crystalline contacts. To this end, even the most careful UHV friction experiment will inevitably measure friction between somewhat non-perfect crystals, complete with a variety of defects, such as surface steps, kinks or reconstructions.

The calculated values in table 2 contain a significant dependence of friction with load. However, one of the most common macroscopic observations is that friction varies little as a function of normal load. In order to account for this, an accurate multi-asperity model is needed for incorporation into the calculations [43,44]. A complete topographic analysis of the surface would allow for the statistical analysis (autocorrelation, roughness, skewness, kurtosis) of asperity heights leading to a more load-independent calculation of friction forces for multi-asperity contacts.

7. Discussion

The model that we have described gives quite reasonable numbers for both the dynamical and static friction coefficient. Many real cases will not be dominated by just the interfacial term that we have considered, but will involve more complicated dislocation motion. Just as plastic deformation of materials at the nanoscale depends on the motion of dislocations which at a continuum level can be represented by, for instance, constituent models, we will argue that the nanoscale understanding of friction *must* involve dislocation motion near the interfaces, which can (in the future) be built up into more continuum scale constitutive frictional models.

We certainly cannot as yet explain all frictional phenomena, but there are a number of cases where there are some relatively straightforward connections between our model and existing experimental data. In addition, since dislocation models have primarily been developed for strong materials, there are some open issues when it comes to the relatively weak interfaces that one probably has in most real cases of friction. There are also some open questions, for instance when interface dislocations are moving faster than the speed of Rayleigh

Table 2.
Comparison of experimental and theoretically calculated friction coefficients.

	Σ	L	**b**, $\lvert b_{hkl}\rvert$ [Å]	$\lvert \mathbf{v}_d\rvert$ m/s	N	T (K)	μ_{exp}	μ_{calc}	Ref.
Fe(100)			2.87		0.1–0.15N		5.8 ± 1.1		59
	1	5		1.05E-04	0.1–0.15N	300		92.82–106.3	
	1	25		5.23E-04	0.1–0.15N	300		11.14–17.00	
	5	5	1/10 < 310 >	1.05E-03	0.1–0.15N	300		9.28–10.62	
	5	25	1/10 < 310 >	5.23E-03	0.1–0.15N	300		1.11–1.69	
	25	5	1/25 < 430 >	2.61E-03	0.1–0.15N	300		3.71–4.25	
	25	25	1/25 < 430 >	1.31E-02	0.1–0.15N	300		.45–.67	
Cu(111)			2.55		25–50 mN	100	7.8 ± 1.8		45
	1	5		3.92E-04	25–50 mN	100		275.1–346.6	
	1	25		1.96E-03	25–50 mN	100		11.0–13.86	
	5	5	1/10 < 310 >	3.92E-03	25–50 mN	100		27.51–34.67	
	5	25	1/10 < 310 >	1.96E-02	25–50 mN	100		1.10–1.39	
	25	5	1/25 < 430 >	9.80E-03	25–50 mN	100		11.0–13.86	
	25	25	1/25 < 430 >	4.90E-02	25–50 mN	100		0.44–0.55	
Ni(100)			3.52		40 mN	300	8.6 ± 2.5		51
	1	5		2.84E-04	40 mN	300		495.66	
	1	25		1.42E-03	40 mN	300		31.72	
	5	5	1/10 < 310 >	2.84E-03	40 mN	300		49.568	
	5	25	1/10 < 310 >	1.42E-02	40 mN	300		3.172	
	25	5	1/25 < 430 >	7.10E-03	40 mN	300		19.833	
	25	25	1/25 < 430 >	3.55E-02	40 mN	300		1.2694	

Ranges displayed in μcalc correspond to the values calculated for the experimental range of loads. Σ is the coincident site boundary (CSL) index, L is the inter-dislocation spacing in nanometers, **b** is the burgers vector and $|b|$ its magnitude in Angstroms, v_d is the dislocation velocity orthogonal to the burgers vector in m s^{-1}, N is the normal force, μ_{exp} is the experimental kinetic friction coefficient and μ_{calc} is the calculated friction coefficient from the dislocation drag model.

waves at the interface, which merit further investigation. This discussion presents a collection of tribological phenomena that can be directly understood and explained through this model, as well as some potential topics for future research.

7.1. Superconducting transition

The effect of superconductivity on friction has recently been studied by Dayo *et al*. [61] and Renner *et al* [62] in systems of sliding monolayer films on lead substrates using a QCM. Dayo *et al*. presented evidence of a sudden decrease in friction for N_2 films sliding on Pb substrates as the superconducting transition is crossed. In an attempt to reproduce this experiment, Renner *et al*. observed a pinned film, with no slip occurring at any of their experimental conditions. It was concluded by the authors that slight differences in laboratory conditions (humidity and substrate preparation consistency) are to blame for the disparate results [62]. In the viewpoint of our model, both results are valid, and even predicted. In the case of the pinned film, the Peierls relief barrier is sufficiently large so that the effects of electronic drag are not measured. This can result from the presence of dislocations or steps at the interface, which can act as dislocation sources as discussed later in this work, and is within the error of sample preparation techniques. A step free interface will not include these additional barriers, enabling slip and the measurement of the friction force.

At low temperatures phonon modes are "frozen out", allowing electronic drag contributions to play a more significant role. However, when the superconducting transition is crossed, the number of electrons interacting with dislocations is substantially smaller. It has been shown both theoretically [39] and experimentally [34,36–38] that the plastic properties, namely dislocation drag, are greatly affected by crossing the superconducting transition. Detailed mathematical expressions for the form of drag can be found in works by Kaganov and Natsik [63] and Huffman and Louat [39]. Interestingly, for the case of dry friction, these calculations demonstrate that for $v \ll v_c$ the electron drag coefficient B_e is no longer constant under the superconducting transition temperature. Furthermore, it follows the temperature dependence of the normal electron density. This was confirmed experimentally by Kobelev and Soifer [64] in a bulk material, and is worthy of further investigations regarding solid friction experiments at low temperatures.

7.2. The Aubry transition and superlubricity

As pointed out some time ago by Aubry [65], for certain special, weakly bonded incommensurate interfaces the dislocations dissociate and the nominal static friction coefficient goes to zero. The dynamical friction due to traveling strain fields at the interface will not vanish, so there will still be a contribution although we are not aware of any attempts to apply the established drag models to this specific case. The concept of *superlubricity*, a dramatic reduction of the static friction force, has been the subject of much controversy since its definition in a work by Shinjo and Hirano [66]. It was shown, albeit not conclusively, in both experiments and simulations that some conditions will lead to a decrease in the friction force by several orders of magnitude by simply changing the relative orientation of a crystalline contact [67,68]. The scanning probe study, however, fails to directly measure a normal force, and, strictly speaking, only establishes a tunneling ‚contact'. A more careful FFM study by Dienwiebel [48] has shown very low sliding friction forces between graphite flakes under extremely low loads. The original definition of *superlubricity* only accounts for dissipative elements associated with phonons. Radiation friction and electronic drag terms, as described in the introduction do not necessarily behave in the same way as to vanish upon forming an incommensurate contact. All sliding contacts will contain some type of defect, whether it is due to finite size (edge) effects or due to larger scale lattice relaxations that give rise to misfit dislocations. The exact nature of the defect will determine its Peierls barrier that will produce a finite friction force. Even in the case of graphite, where the Peierls barrier in the basal plane was determined to be 1×10^{-17} Pa, an exceedingly small but finite friction force exists [55,69]. This extremely small dislocation barrier in the graphite basal plane suggests that other defects or surface terminating layers play the most significant role in friction for this system. Pinning at the ends containing a dislocation line tension is likely to dominate sliding of layers in graphite. This is considered to be the stress required to multiply dislocations at Frank–Read sources. The origins of the low tribological properties of graphite must not be viewed as sudden shifts of entire basal planes over one another, but as the incremental propagation of dislocations throughout the interface [69]. A calculation using our model has been carried out to reproduce conditions given in the experiment by Dienwiebel [48] (F_N = 18 nN, V = 20 nm/s, R = 80 nm), with shear stress values for single-crystal graphite measured by Soule and Nezbeda [70] (σ = 29 kPa). We arrive at a Σ1 friction range of μ = 0.001–0.026 for dislocation spacing limits of 5 and 25 nm. The value reported for Dienwiebel's FFM experiment in the case of commensurate (near Σ1) contact, was μ = 0.017, clearly consistent with the calculated results.

Since intrinsic grain boundary dislocations can be pushed out of an interface by applying a shear stress (in this case, sliding), sources for additional dislocations must exist as well to maintain a dynamic friction force.

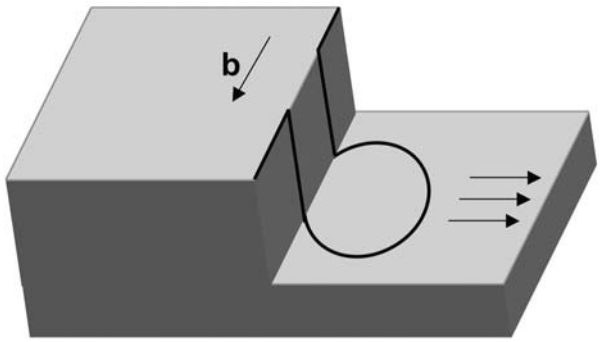

Figure 8. A Koehler dislocation source. A screw dislocation cross-slips to a new plane before continuing motion on the original slip system. Multiplication of dislocations can occur in this manner at a stepped interface.

Steps on a crystal surface can act as sources of dislocations, via the Koehler mechanism [71]. Similar to a Frank-Read source [72], this process of moving a screw dislocation to an intersecting plane (cross-slip) can lead to the multiplication of dislocations as drawn schematically in figure 8. Pile-up of dislocations will result, preventing further motion in the slip plane. The angular distribution of burgers vectors is changed by this process, altering the anisotropic behavior of the retarding force.

7.3. Third bodies and transfer layers

In the large majority of cases, one must allow for the existence of third body sliding in the analysis of most friction experiments. In the present context of dislocation-mediated friction, a third body can be modeled as two sliding interfaces rather than one, each interface (and the respective interface dislocations) moving at half the speed. In the high velocity regime of our model the net dissipative force will be unchanged, but in the lower velocity regimes it will be increased by a factor of two, assuming a constant density of dislocations. Of course, if the third body has a substantially lower Peierls stress then the dominant sliding mechanism will be via dislocations standing off from the interface. This well-characterized phenomenon [73–75] can be directly applied to solid friction experiments, correlating wear of a transfer layer to the stand-off distance of dislocations during sliding. Mader and Knauss have shown in both experiment and theory that dislocation standoff for the metal-oxide interface between Nb and Al_2O_3 is between 1.8 and 4.0 d_{110} spacings. For materials with highly dissimilar shear moduli, it is not unreasonable to have standoff distances exceeding 20 planar spacings. In our model this would correlate with the width of any transfer layers. This we consider to be a relevant wear mechanism for solid lubricants (graphite, MoS_2).

7.4. Work hardening and stick slip

It is interesting that the dislocation model will give a form of stick-slip behavior at a more nanoscale level, as against at the atomic level. Orderly motion of dislocations as we have assumed (for simplicity) rarely occurs in practice, instead one often gets what are called dislocation tangles due to the effects of barriers in the material. For the case of friction this would be anything from surface steps to surface impurities. As the dislocations become entangled, the density of dislocations increases and the stress to move them becomes higher, what is called cold work; this is a bulk phenomenon, but we see no reason why it should not also occur at a surface. The higher stress level required to move the dislocations can lead to a different path for sliding to become activated, in effect a stick-slip process.

7.5. Supersonic dislocations

One area where there might be some new effects is the regime, where dislocations are moving at close to or above the local speed of sound. The governing elastic equations are analogous to the equations of relativity, with the local speed of sound replacing the speed of light in vacuum, with the exception that physically realistic solutions do occur above the speed of sound. Elasticity theory for dislocation drag has solutions for supersonic motion, but at stresses that significantly exceed critical yield stresses of materials when the shear wave velocity is approached. More recent atomistic models have shown that sustained supersonic dislocation motion is possible given a supersonic starting condition [76,77]. At an interface, particularly a relatively weak one, the interfacial speed of sound (corresponding to Love or Rayleigh waves) can be easily exceeded, and there might well be new physical phenomena.

7.6. Collective dislocation modes: superplasticity

Grain boundary sliding refers to the displacement of individual grains past one another when a sufficient external stress is applied. This is equivalent to all the misfit dislocations at the boundary moving collectively, as against single dislocation motion. The relative motion of the grains can take place immediately at the interface, or at some small standoff distance (e.g., buffer layers) from the boundary. In bulk materials this type of deformation process leads to what is called superplasticity where plastic strain elongation can reach several hundred percent (even up to 1000%) before failure. It has been shown by internal friction experiments that twist boundaries with higher energy are more susceptible to grain boundary sliding than those with low Σ indecies [78], which is predicted by

our model. Two basic conditions are required to achieve superplastic behavior: (1) grain sizes typically less than 10 μm and (2) high temperatures, usually at least half of the melting temperature. In nanocrystalline materials grain boundary sliding is often the dominant mode of deformation.

We will speculate that a similar phenomenon may be responsible for some solid lubricants at elevated temperatures; at lower temperatures, we expect superplastic effects to occur for polymers or self-assembled monolayers. These processes (in the bulk) are often thermally activated, so a careful analysis of the temperature dependence could potentially prove (or disprove) our hypothesis.

7.7. Non-metallic friction

Covalent materials typically have Peierls stress values many times higher than for metals. Experimentally, however, lower friction forces are measured for nonmetals than for metals in almost every case. Buffer layers and dislocation standoff explain this discrepancy. The formation of native oxide layers or passivation layers at surfaces changes the magnitude in which interfacial dislocations interact to produce a drag force. Small standoff distances from an interface (a few Angstroms) will cause a decrease in the drag stress, since the dislocation now rests in the softer material. Also, native passivation layers are typically amorphous, which can more easily lead to incommensurate contact conditions, known to decrease friction [10,13,50,51,79].

8. Conclusions

We have developed an analytical friction model by combining known theories of interfaces, dislocations, and contact mechanics. Using no adjustable parameters, only basic materials constants and given experimental conditions, we demonstrate agreement between magnitudes of calculated friction values and experimental UHV friction data indicating that dislocation motion is an important mechanism in the analysis of crystalline sliding contacts. The model directly addresses temperature, velocity and anisotropic dependence, showing that friction behaves analogously to how dislocations are affected by these factors. A number of tribological phenomena may be understood through this model, including superconducting friction, supersonic dislocation motion, buffer layers and dislocation stand-off as an atomic wear mechanism, superlubricity and the formation of work-hardened tribolayers from dislocation pile-up at Koehler sources. Ample room exists to exploit the suggested phenomena through experiments at temperature extremes and at high velocities for crystalline friction.

References

[1] D. Dowson, *History of Tribology (Professional Engineering Publishing, London, 1998)*.
[2] J.P. Gao, W.D. Luedtke and D. Gourdon et al., J. Phys. Chem. B 108 (2004) 3410.
[3] G. Binnig, C.F. Quate and C. Gerber, Phys. Rev. Lett. 56 (1986) 930.
[4] C.M. Mate, G.M. McClelland and R. Erlandsson et al., Phys. Rev. Lett. 59 (1987) 1942.
[5] J. Krim, D.H. Solina and R. Chiarello, Phys. Rev. Lett. 66 (1991) 181.
[6] E.T. Watts, J. Krim and A. Widom, Phys. Rev. B 41 (1990) 3466.
[7] D. Tabor and Rh Winterto, Proc. R. Soc. Lond. Ser. a-Math. Phys. Sci. 312 (1969) 435.
[8] G.A. Tomlinson, Philos. Mag. 7 (1929) 905.
[9] T. Kontorova and Y. I. Frenkel (1938) Zh Eksp Teor Fiz 8.
[10] M. Weiss and F.J. Elmer, Z. Phys. B-Condens. Matter 104 (1997) 55.
[11] F. Frank and J.H. van der Merwe, Proc. R. Soc. Lond. Ser. A 198 (1949) 205.
[12] F. Frank and J.H. van der Merwe, Proc. R. Soc. Lond. Ser. A 198 (1949) 217.
[13] M. Weiss and F.J. Elmer, Phys. Rev. B 53 (1996) 7539.
[14] J.A. Harrison, C.T. White and R.J. Colton et al., Phys. Rev. B 46 (1992) 9700.
[15] U. Landman and W.D. Luedtke, J. Vac. Sci. Technol. B 9 (1991) 414.
[16] V.I. Alshits, V.L. Indenbom and J. Lothe, *Progress in Materials Science*, 1992)(Elsevier Science, Amsterdam, 1992) 625.
[17] A.P. Sutton and R.W. Balluffi, *Interfaces in Crystalline Materials (Oxford University Press, Oxford, 1995)*.
[18] D. Wolf and S. Yip, *Materials Interfaces: Atomic-level Structure and Properties* (*Chapman and Hall, London, 1992*).
[19] J.M. Howe, *Interfaces in Materials (Wiley, New York, 1997)*.
[20] J. Weertman and J.R. Weertman, *Elementary Dislocation Theory (Oxford University Press, Oxford, 1992)*.
[21] J.P. Hirth and J. Lothe, *Theory of Dislocations (Krieger Publishing Company, Malabar, 1982)*.
[22] E. Barthel, J. Colloid Interface Sci. 200 (1998) 7.
[23] K.L. Johnson, *Contact Mechanics (Cambridge University Press, Cambridge, 1985)*.
[24] W.N. Unertl, J. Vac. Sci. Technol. A 17 (1999) 1779.
[25] W. Bollmann, Philos. Mag. 16 (1967) 363.
[26] W. Bollmann, Philos. Mag. 16 (1967) 383.
[27] H. Grimmer, W. Bollmann and Dh Warringt, Acta Crystallogr. Sect. A A 30 (1974) 197.
[28] G. Leibfried, Z. Phys. 127 (1950) 344.
[29] V.L. Indenbom and A.N. Orlov, in: *Proc. Conf. Dislocation Dynamics*, (Kharkov, 1967) 3.
[30] S.V. Lubenets and V. I. Startsev, Sov Phys Solid State 10 (1968) 15.
[31] V.I. Alshits, Sov. Phys. Solid State, Ussr 11 (1970) 1947.
[32] V.I. Alshits and Y.M. Sandler, Phys. Stat. Sol. 64 (1974) K45.
[33] T. Holstein, Phys. Rev. 151 (1966) 187.
[34] G.A. Alers, O. Buck and B.R. Tittmann, Phys. Rev. Lett. 23 (1969) 290.
[35] H. Kojima and T. Suzuki, Phys. Rev. Lett. 21 (1968) 896.
[36] A. Hikata and C. Elbaum, Phys. Rev. Lett. 18 (1967) 750.
[37] B.R. Tittmann and H.E. Bommel, Phys. Rev. 151 (1966) 178.
[38] W.P. Mason, Phys. Rev. 143 (1966) 229.
[39] G.P. Huffman and N. Louat, Phys. Rev. Lett. 24 (1970) 1055.
[40] V.I. Alshits, A. Shtolberg and V.L. Indenbom, Phys. Status Solidi B-Basic Res. 50 (1972) 59.
[41] K.L. Johnson, K. Kendall and A.D. Roberts, Proc. R. Soc. Lond. Ser. a-Math. Phys. Sci. 324 (1971) 301.
[42] B.V. Derjaguin, V.M. Muller and Y.P. Toporov, J. Colloid Interface Sci. 53 (1975) 314.

[43] J. Greenwood and J.H. Tripp, J. Appl. Mech. 34 (1967) 153.
[44] J. Greenwood and J. Williams, Proc. R. Soc. Lond. Ser. a-Math. Phys. Sci. 295 (1966) 300.
[45] C.F. McFadden and A.J. Gellman, Surf. Sci. 409 (1998) 171.
[46] L. Bureau, C. Caroli and B. Baumberger, Phys. Rev. Lett. 97 (2006) 5501.
[47] D.J. Dingley and R.C. Pond, Acta Metallurgica 27 (1979) 667.
[48] M. Dienwiebel, N. Pradeep and G.S. Verhoeven et al., Surf. Sci. 576 (2005) 197.
[49] T. Gyalog and H. Thomas, Europhys. Lett. 37 (1997) 195.
[50] M. Dienwiebel, G.S. Verhoeven, N. Pradeep, et al., Phys. Rev. Lett. 92 (2004) 126101.
[51] M. Hirano, K. Shinjo and R. Kaneko et al., Phys. Rev. Lett. 67 (1991) 2642.
[52] J.S. Ko and A.J. Gellman, Langmuir 16 (2000) 8343.
[53] Y. Qi, Y.T. Cheng, T. Cagin, et al., Phys. Rev. B 66 (2002) 085420.
[54] Y. Enomoto and D. Tabor, Proc. R. Soc. Lond. Ser. a-Math. Phys. Eng. Sci. 373 (1981) 405.
[55] B. Joos and M.S. Duesbery, Phys. Rev. Lett. 78 (1997) 266.
[56] A.I. Landau, Phys. Status Solidi a-Appl. Res. 61 (1980) 555.
[57] S.E. Babcock and R.W. Balluffi, Philos. Mag. a-Phys. Condens. Matter Struct. Defects Mech. Properties 55 (1987) 643.
[58] T. Schober and R.W. Balluffi, Philos. Mag. 21 (1970) 109.
[59] T.Y. Tan, S.L. Sass and R.W. Balluffi, Philos. Mag. 31 (1975) 575.
[60] B.M. Dekoven and P.L. Hagans, J. Vac. Sci. Technol. a-Vac. Surf. Films 8 (1990) 2393.
[61] A. Dayo, W. Alnasrallah and J. Krim, Phys. Rev. Lett. 80 (1998) 1690.
[62] R.L. Renner, P. Taborek and J.E. Rutledge, Phys. Rev. B 63 (2001).
[63] M.I. Kaganov, Vy Kravchen and V.D. Natsik, Usp. Fiz. Nauk 111 (1973) 655.
[64] N.P. Kobelev and Y.M. Soifer, Phys. Status Solidi a-Appl. Res. 50 (1978) K185.
[65] S. Aubry and P.Y. Ledaeron, Physica D 8 (1983) 381.
[66] K. Shinjo and M. Hirano, Surf. Sci. 283 (1993) 473.
[67] M. Hirano, K. Shinjo and R. Kaneko et al., Phys. Rev. Lett. 78 (1997) 1448.
[68] M. Hirano and K. Shinjo, Wear 168 (1993) 121.
[69] R.H. Telling and M.I. Heggie, Philos. Mag. Lett. 83 (2003) 411.
[70] D.E. Soule and C.W. Nezbeda, J. Appl. Phys. 39 (1968) 5122.
[71] J.S. Koehler, Phys. Rev. 86 (1952) 52.
[72] F.C. Frank and W.T. Read, in: *Symposium on Plastic Deformation of Crystalline Solids*, (Carnegie Institute of Technology, Pittsburgh, 1950) 44.
[73] S.V. Kamat, J.P. Hirth and B. Carnahan, in: *MRS Symposia Proceedings*, Vol. 103, ed. T. W. Barbee Jr. (Pittsburgh, 1988) 55.
[74] W. Mader, Mater. Res. Soc. Sym. Proc. 82 (1987) 403.
[75] W. Mader and D. Knauss, Acta Metall. Mater. 40 (1992) S207.
[76] P. Gumbsch and H. Gao, Science 283 (1999) 965.
[77] P. Gumbsch and H.J. Gao, J. Comput. Aided Mater. Des. 6 (1999) 137.
[78] M. Kato and T. Mori, Philos. Mag. A 68 (1993) 939.
[79] M. Cieplak, E.D. Smith and M.O. Robbins, Science 265 (1994) 1209.